

## Variation in colloidal chromophoric dissolved organic matter in the Damariscotta Estuary, Maine

Sheri A. Floge<sup>1</sup>

Darling Marine Center, University of Maine, 193 Clarks Cove Road, Walpole, Maine 04573-3307

Mark L. Wells

Darling Marine Center, University of Maine, 193 Clarks Cove Road, Walpole, Maine 04573-3307; School of Marine Sciences, University of Maine, 5741 Libby Hall, Room 214, Orono, Maine 04469-5741

### Abstract

The relationship between chromophoric dissolved organic matter (CDOM), colloidal DOM (>1 kDa), and phytoplankton biomass in marine waters of the Damariscotta estuary, Maine, was studied using flow field-flow fractionation (flow FFF). The goal was to determine whether temporal variability in CDOM in this region is due in part to rapid cycling of marine colloids. CDOM absorption of filtered (0.2  $\mu\text{m}$ ) seawater correlated positively with colloidal absorbance ( $r^2 = 0.772$ ,  $p = 0.021$ ). We observed changes in colloidal size spectra and CDOM optical properties associated with phytoplankton biomass. In particular, a significant positive correlation was found between the <18 kDa colloidal fraction and chlorophyll *a* (Chl *a*) ( $r^2 = 0.819$ ,  $p = 0.013$ ). While we did not find significant relationships between Chl *a* and either CDOM absorption or the spectral slope of filtered seawater ( $r^2$  and  $p$  values of 0.079, 0.590 and 0.111, 0.519, respectively), we did observe patterns of higher CDOM absorption and spectral slopes following periods of increased phytoplankton biomass. The spectral slope of colloidal material often was significantly lower than that of filtered seawater and normally varied significantly with colloidal size. These findings show that colloidal processes can contribute to CDOM optical signatures in coastal waters.

Chromophoric dissolved organic matter (CDOM) is the collective name for a diverse assemblage of organic compounds dissolved in aquatic environments that absorb light in the ultraviolet (UV) and visible domains (Jerlov 1976). These compounds comprise a significant but highly variable fraction of the total dissolved organic matter pool (Thurman 1985, and references within) and play an essential role in biogeochemical cycles, microbial ecology, and the determination of optical properties in marine surface waters. Specifically, CDOM may directly limit the penetration of both UV and photosynthetically active radiation (Blough and Del Vecchio 2002, and references within), influence nutrient and trace metal availability (Blough and Del Vecchio 2002, and references within), and undergo photochemical transformations to produce trace gases, CO, CO<sub>2</sub> (Nelson and Siegel 2002, and references within), harmful reactive oxygen species (Miller 1994; Blough and Zepp 1995), and biologically labile organic compounds (Kieber et al. 1989).

Both the abundance and the spectral signature of CDOM in marine waters are highly variable and do not covary predictably with chlorophyll *a* (Chl *a*), phytoplankton cell numbers, or dissolved organic carbon (DOC)

(Siegel and Michaels 1996; Nelson et al. 1998). Although the influence CDOM exerts on upper ocean processes is well recognized, the dynamics of these compounds remain largely undefined. Coastal regions in particular display high spatial and temporal variability in CDOM abundance and optical characteristics (e.g., Nelson and Guarda 1995; Vodacek et al. 1997), which can interfere with satellite-based estimates of phytoplankton biomass and contribute signal in other remote sensing applications (Carder et al. 1989; Hochman et al. 1994; Siegel and Michaels 1996).

Oceanographers traditionally have separated seawater constituents into dissolved and particulate phases by filtration through 0.2–0.7- $\mu\text{m}$  pore sized filters; however, 30–70% of dissolved organic carbon actually is colloidal (1–1,000 nm) (Benner et al. 1992; Guo et al. 1994; Buesseler et al. 1996). Colloids 400–1,000 nm in size occur at  $\sim 10^7$  particles mL<sup>-1</sup> (Koike et al. 1990; Longhurst et al. 1992), and smaller colloids (5–200 nm) are found at concentrations of  $>10^9$  particles mL<sup>-1</sup> (Wells and Goldberg 1991, 1992, 1994). The colloidal phase can contain a significant portion of the chromophoric substances in seawater (Wells unpubl. data), and the spectroscopic properties of colloidal matter differs from that of truly dissolved CDOM (Mopper et al. 1996; Boehme and Wells 2006).

Rapid biogeochemical cycling of colloids in marine surface waters (Baskaran et al. 1992; Moran and Buesseler 1992) suggests that the concentrations of colloidal CDOM may vary on short time scales, potentially altering bulk seawater CDOM optical characteristics. Marine colloidal matter frequently covaries with biological parameters such as Chl *a* and bacterial numbers (Koike et al. 1990; Wells and Goldberg 1994; Yamasaki et al. 1998), suggesting that

<sup>1</sup> Corresponding author (sheri.floge@maine.edu).

### Acknowledgments

We thank Mary Jane Perry for use of the phytoplankton culturing facilities and Remy Luerrson and Emily Kallin for the chlorophyll data used in this study. This work was supported by the Office of Naval Research (ONR N00140010304). We appreciate the constructive comments provided by two anonymous reviewers.

colloid abundance, composition, and dynamics will be strongly influenced by biological processes. In particular, small colloidal material (1–200 nm) may be derived from phytoplankton either directly through the sloughing off of materials from the cell and organic matter exudation or indirectly through viral lysis and grazing (Wells and Goldberg 1994). Indeed, algal exudation of metabolites has been well documented (e.g., Hellebust 1965; Baines and Pace 1991) and may account for up to 40% or more of photosynthetically produced organic carbon (Sundh 1989). The chromophoric characteristics of these substances as a function of size remain largely unknown.

The study of colloids and their size distributions in seawater has been achieved using such diverse methods as membrane ultrafiltration (Zsolnay 1979), resistive-pulse particle counting (Koike et al. 1990), laser-light scattering (Chin et al. 1998), transmission electron microscopy (Harris 1977; Wells and Goldberg 1991, 1994), and atomic force microscopy (Santschi et al. 1998). Flow field-flow fractionation (flow FFF) is a novel approach to the separation of marine colloidal matter by molecular size (Beckett and Hart 1993; Hasselhov et al. 1996). Flow FFF is a chromatography-like analytical separation technique that separates colloids based on their diffusion coefficient (Giddings 1993). One of the major advantages of flow FFF is the ability to obtain a continuous size spectrum of colloidal matter that may then be analyzed by various in-line detectors (e.g., UV–Visible [Vis] spectrophotometers, fluorometers) or collected for analysis by other techniques.

We applied flow FFF to examine changes in colloidal size and associated optical properties of CDOM at a coastal site over a period of 2 yr. We sought to determine the extent that the optical signature of marine colloidal matter varied in response to phytoplankton abundance. Specifically, we measured the size distribution of colloids in the range of ~1–40 nm and the absorbance spectra (200–700 nm) of both filtered seawater (0.2  $\mu\text{m}$ ) and colloidal size fractions in the Damariscotta estuary, Maine, on a roughly bimonthly basis. This work was conducted in conjunction with an investigation of colloidal fluorescence variability reported elsewhere (Boehme and Wells 2006).

## Methods

*Flow field-flow fractionation*—Theory: Flow FFF combines elements of chromatography and field-driven techniques, such as electrophoresis, to achieve separation based on particle diffusion coefficients (Giddings 1993). Two independent flow streams are superposed at right angles to one another within a thin ribbonlike channel having a total volume of ~1.2 mL. The flow along the long axis of the channel (channel flow) is laminar, has a parabolic profile, and sweeps particulate material toward the outlet. The cross flow stream, entering and exiting through permeable ceramic frit walls, drives particles toward a membrane cutoff filter covering one side of the channel (the accumulation wall). Brownian motion of the colloids opposes the cross flow and leads to a concentration cloud that extends up from the accumulation wall. At equilibrium, smaller colloids (i.e., having higher diffusion

coefficients) will extend farther above the accumulation wall than larger colloids and thus be advected faster along the channel by the parabolic laminar flow (see fig. 1 in Boehme and Wells 2006). Particle retention time within the channel can be related precisely to the particle's diffusion coefficient through mathematical relationships. The diffusion coefficient is used to estimate particle diameter through the Stokes–Einstein equation. Molecular weight standards are used to establish the relationship between elution time and colloid diameter (Ratanathanawongs and Giddings 1993; Vaillancourt and Balch 2000). See Giddings (1993) for a review of flow FFF theory and Giddings et al. (1976, 1977) for mathematical treatment of size separation by flow FFF.

*Experimental system*: The experimental setup consisted of a F-1000-FO universal fractionator (Postnova Analytics) that was modified for on-channel preconcentration. The channel assembly comprised two acrylic blocks with ceramic frits, between which was placed a regenerated cellulose membrane (Postnova Analytics) having a nominal molecular weight cutoff of 1,000 Daltons (ca. 1 nm equivalent spherical diameter) and a 254- $\mu\text{m}$  thick polyester spacer (Postnova Analytics). The channel dimensions were 29.4 cm long (tip to tip), 2.0 cm wide, and nominally 0.0254 cm thick. Both the channel flow and cross flow were controlled by Series II digital pumps (LabAlliance). Teflon tubing connected all the components, and a Rheodyne model 7725 injector (Alltech Associates) was used for sample injection. A recirculated cross flow stream was used to maintain a uniform cross flow force field. Channel flow exited the channel at two points at the end of the channel block: at the outlet to the detector and, just upstream, at the frit outlet. The frit outlet is designed to concentrate the sample components eluting from the channel by diverting part of the carrier flow above the accumulation wall, through the permeable frit material. Relative flow through the frit outlet and to the detector was controlled with a needle valve that enabled enrichment of the sample with colloids prior to detection by the UV–Vis absorbance detector (model VUV-10, HyperQuan).

This method estimates colloid abundance by absorbance of UV light and therefore may underrepresent poorly UV-absorbing colloidal matter (see *Discussion*). The detector sensitivity setting was 0.05 absorbance units (AU) and absorbance was measured at 254 nm. The outflow from the UV–Vis detector was interfaced to a long pathlength liquid core waveguide (LWCC-2; WPI, World Precision Instruments) for determination of absorbance spectra (200–700 nm) of colloidal size fractions. Software supplied with the F-1000-FO (FFFAnalysis) controlled cross flow pump rates, recorded the detector analog response, and was used to obtain retention time, peak height, and peak area. The FFFAnalysis software converts UV–Vis detector voltage into response counts, a unitless number that then can be related to absorbance units based on the detector settings. Colloidal CDOM absorbance (254 nm) data presented here are approximately  $\times 10^{-4}$  AU.

*Operating conditions*: The carrier solution was artificial seawater (Aquil; Morel et al. 1979; Price et al. 1989) with a salinity of 32 and a pH of 8.1. Carrier solutions were

prepared within 1–2 d of use in the system. Artificial seawater, ultrafiltered natural seawater, and phosphate buffer solution (sodium phosphate [Sigma-Aldrich] in deionized water, pH 8.0, 1 mol L<sup>-1</sup>) were tested to determine the effect of carrier solutions on natural colloid size distribution. No difference was found between colloidal size spectra of samples run in artificial seawater and ultrafiltered natural seawater. However, the phosphate buffer carrier solution caused an apparent decrease in natural colloid size. Artificial seawater was chosen as the carrier solution to avoid complications from CDOM present in natural seawater. We did not add surfactants to the carrier solution to minimize potential disruption of proposed calcium and magnesium cross-linking bonds in natural colloids (Chin et al. 1998).

The channel and cross flow rates were held constant at 2.0 and 4.0 mL min<sup>-1</sup>, respectively. A backpressure regulator (689 kPa, Upchurch Scientific) and a 15 cm length of PEEK (polyetheretherketone) tubing was placed after the detector to improve baseline stability and to avoid cavitation inside the recirculating reservoir. The system pressure ranged from 724 to 793 kPa. Fifty milliliter samples were concentrated on-line according to the procedure of Lyven et al. (1997), whereby sample is pumped backward into the channel through the channel outflow port while carrier is introduced through the channel inflow port. Preconcentration of colloids was achieved using a forward:backward channel flow ratio of 0.1:1.2 mL min<sup>-1</sup> for 48 min and 40 s. Samples then were run under normal operating conditions for 40 min. A 50-mL sample of carrier solution was run at the beginning of each set of samples to test for system or carrier solution contamination. Colloidal size distribution samples were typically run in triplicate. These operating conditions enabled separation of colloids in the approximate size range of 1–400 kDa or 1–40 nm based on equivalent spherical diameter. Although we clearly are sampling only the smallest size fraction of the total colloidal material (i.e., 1–40 nm vs. 1–1,000 nm diameter) for simplicity we refer to this fraction as total (measured) colloidal material in the text.

Small variations in channel thickness arise when the channel is opened for cleaning or the membrane is replaced. Experimental determination of channel thickness and volume was conducted after channel disassembly for cleaning and periodically during time series experiments to assess stability of the system. The thickness of the channel ( $\omega$ ) was determined using bovine serum albumin (BSA, Sigma-Aldrich) dissolved in artificial seawater to a concentration of 1 mg mL<sup>-1</sup>. The standard was run under normal operating conditions, and the thickness of the channel was determined with the equation:  $\omega_{\text{new}} = ((d_{\text{app}})(\omega_{\text{app}})^2(d_{\text{act}}))^{-0.5}$  where  $\omega_{\text{new}}$  is the new thickness of the channel,  $d_{\text{app}}$  is the apparent diameter of the BSA,  $d_{\text{act}}$  is the actual diameter of the BSA (7 nm), and  $\omega_{\text{app}}$  is the apparent thickness of the channel as determined by previous calibrations. Following determination of channel thickness, the void volume of the channel is recalculated using the equation:  $V_0 = bL_v\omega_{\text{new}}$  where  $V_0$  is the new channel volume,  $b$  is the channel width,  $L_v$  is the channel length, and  $\omega_{\text{new}}$  is the channel thickness.

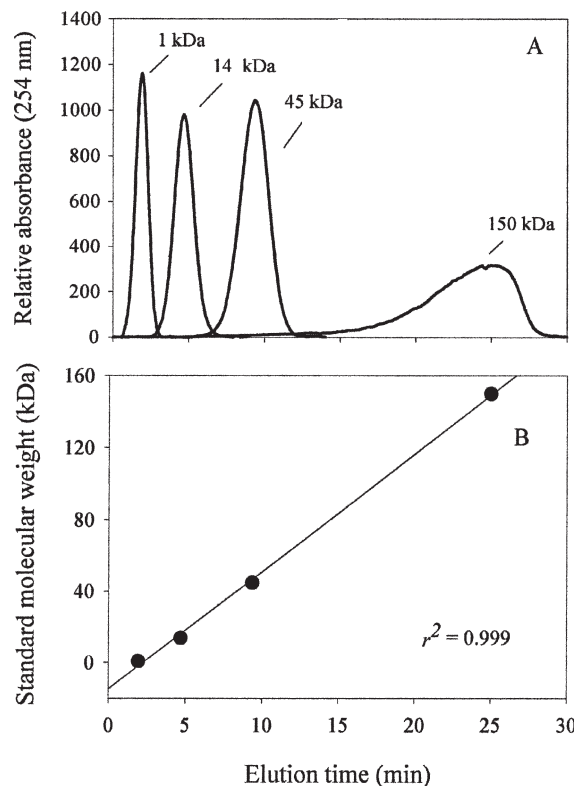


Fig. 1. Size separation of molecular weight standards by flow FFF. (A) Flow FFF fractogram. Each line is the mean of three replicates. Maximum percentage relative standard deviation for peak elution time of standards was 2.4%. (B) The relationship between elution time from flow FFF channel and molecular weight. The mean elution times of three replicates are shown for molecular weight standards sized 1, 14, 45, and 150 kDa. Error bars representing one standard deviation are smaller than the symbol size. The coefficient of determination,  $r^2$ , is shown.  $x$ -axes are identical; note different scales on  $y$ -axes.

Polystyrene sulfonate sodium salt (PSS) standards (Polymer Standards Service) with peak molecular weights of 1.09, 6.71, 14.00, 45.10, 82.80, and 150.00 kDalton (kDa) were used to generate calibration curves relating elution time to peak molecular weight (Fig. 1). These provided a means for approximating molecular weights of natural colloids. Standards were dissolved in artificial seawater to a concentration of 1 mg mL<sup>-1</sup> and allowed to sit overnight at 4°C prior to use. The absorbance of all PSS standards was monitored at 254 nm, and the system conditions used for the standard runs were identical to those used to analyze environmental samples. On-line concentration was not routinely performed with PSS standards.

Colloidal size distribution data corrections: FFFAnalysis software (Postnova Analytics) enables quantification of colloidal abundance by peak area. The total abundance and that of size fractions <18 kDa, 18–150 kDa, and >150 kDa were determined on replicate seawater samples (two to three replicates). Void peak removal and baseline corrections were performed prior to peak area and height (amplitude) determinations. The amount of error associated with these two data corrections (operator error)

Table 1. Estimates of colloidal size distribution data error. Percentage relative standard deviation for void peak removal and baseline corrections of flow FFF fractograms (operator error) and of replicate samples for the two characteristic colloidal peaks observed.

Peak parameter	%RSD operator error	%RSD replicate error
Small peak elution time	3.18	7.52
Small peak amplitude	2.15	12.0
Small peak area	3.63	14.9
Large peak elution time	0.79	5.22
Large peak amplitude	1.02	10.4
Large peak area	1.25	15.1

was quantified by correcting data from four separate sampling dates and quantifying peak elution time, peak area, and amplitude for each data set three separate times. A comparison between the error due to void peak removal and baseline fixing and the maximum error associated with replicate sample analyses is shown in Table 1. Operator error was found to be significantly less than differences between sample replicates.

*Absorption determinations*—Long pathlength liquid core waveguide/spectrophotometer setup: A type II long pathlength liquid core waveguide (LWCC-2; WPI) was interfaced directly to the flow FFF system for measuring the absorption spectra (200–700 nm) of the different colloidal size fractions. The LWCC-2 capillary cell had a 0.5-m physical pathlength, a 550- $\mu\text{m}$  inner diameter and a cell composed of fused silica tubing with an outer coating of low refractive index polymer (Teflon AF). The waveguide cell is coiled into a 10-cm diameter coil and has standard ST fiber-optic connectors that attach to external optical fibers. The source light, a Xenon flash lamp within the Cary-50 spectrophotometer (Varian), is axially introduced into the waveguide via a 1-m long 400- $\mu\text{m}$  diameter fiber-optic cable (WPI). Light that is transmitted through the sample (i.e., not absorbed or lost to scattering) within the waveguide is collected by a second identical fiber-optic cable and returned to the spectrophotometer for absorbance measurements. A Cary-50 fiber-optic dip probe coupler (Varian) was used to connect the fiber-optic cables to the spectrophotometer. The spectral range of the Cary-50 is 190–1,100 nm, the spectral resolution is 0.15 nm, and the detection range is 0.0005–3 absorbance units (AU). The effective optical pathlength of the LWCC-2 capillary cell was determined to be 0.4837 m with a holmium wavelength calibration standard (Sigma-Aldrich) following the procedure of Belz et al. (1999). The standard, 15% weight/volume in perchloric acid arrived in a sealed glass ampule, was diluted 100-fold with deionized water (Milli-Q, Millipore), and was stored in an amber glass bottle at room temperature.

Bulk filtered seawater CDOM samples (<0.2  $\mu\text{m}$ ) were introduced to the capillary cell via a sample injector kit (WPI). Consistent injection of samples into the capillary cell was achieved using a peristaltic pump pulling the sample through the cell at a speed of 1 mL min<sup>-1</sup>. Samples

were stored in clean glass vials prior to absorbance measurements. The high sensitivity of liquid core waveguides requires that the capillary cell be devoid of cell wall contaminants and microbubbles in order to obtain accurate baseline and absorbance spectra. The capillary cell was cleaned by flushing with a sequence of laboratory detergent (Cleaning solution concentrate, WPI), high reagent grade methanol, 2 mol L<sup>-1</sup> HCl, and deionized water. The cleaning solutions were pulled sequentially through the capillary cell with the peristaltic pump set on maximum pump speed.

Absorbance spectra obtained with the Cary-50 spectrophotometer were determined between 200 and 700 nm at 1-nm intervals relative to an internal reference. Absorbance spectra of replicate deionized water samples were collected at the start of each experiment until the average baseline offset (apparent optical density offset between 680 and 700 nm) of four spectra was less than 0.004 AU. The deionized water absorbance spectra were then saved as a reference spectrum or baseline file and subtracted from all subsequent absorbance spectra obtained that day. Absorbance spectra of fresh deionized water samples were collected throughout the day to check for cell wall contamination.

*Absorbance data corrections:* Occurrence and magnitude of baseline offsets were minimized through avoidance of bubble introduction into the capillary cell. Absorbance spectra with baseline offsets over 0.004 AU were rejected. When baseline offsets were observed, the cell was flushed with 2 mol L<sup>-1</sup> HCl at maximum pump speed while running an absorbance scan. The pump was stopped once the baseline returned to its original value. The cell was then flushed with deionized water prior to measuring sample absorbance spectra.

The spectral absorption coefficients,  $a(\lambda)$  (m<sup>-1</sup>) were obtained using the relationship  $a(\lambda) = 2.303A(\lambda) \times L^{-1}$ , where  $A(\lambda)$  is the absorbance at wavelength  $\lambda$  and  $L$  is the effective optical pathlength in meters. The spectral slopes,  $S$  (nm<sup>-1</sup>), of seawater samples were determined by fitting a single exponential model to the absorption spectrum by the nonlinear least-squares method. The exponential fit was applied by the nonlinear least-squares minimization routine `fminsearch` in Matlab ([www.mathworks.com](http://www.mathworks.com)). The routine conducts an iterative search for the minimum function starting with best guess values for the absorption, slope, and baseline offset. The best guess values used in our model fits were absorption at 400 nm, 0.014 nm<sup>-1</sup>, and 0 m<sup>-1</sup>, respectively. CDOM slopes,  $S$ , were calculated between 316 and 500 nm, the spectral range in which the model best fit the data collected. The extent to which the model fit the data was examined for every sample (by looking at the residuals), including every colloidal size fraction. This precaution was taken to ensure that our model fit the data despite large variations in CDOM absorption among different colloidal size fractions. All regressions and significance values ( $r^2$  and  $p$ ) were calculated using a type II least-squares linear regression with 95% confidence intervals ( $\alpha = 0.05$ ).

*Sample collection*—Surface seawater of the Damariscotta estuary was sampled from the dock at the Darling

Marine Center, University of Maine, Walpole, Maine, on a roughly bimonthly schedule between June 2002 and March 2004. The goal was to capture periods of both high and low phytoplankton biomass in each season. The study area is tidally influenced and does not have significant freshwater input. Over the duration of the study the salinity of surface waters remained above 30, indicating minimal direct freshwater influence on our samples. Although there is considerable tidal advection of water in the Damariscotta estuary, our tests showed that the tidal cycle had little influence on colloidal size distributions (*see Results and Discussion*).

Surface seawater samples were collected below the surface microlayer in acid-washed glass bottles and kept in the dark. Samples were drawn into clean (RBS 35 detergent, Pierce) 60-mL polypropylene syringes (Fisher Scientific) and filtered through prerinsed 0.2- $\mu\text{m}$  low protein binding Durapore (PVDF) syringe filters (Millipore) directly into the online flow FFF concentration sample loop. Syringes were tested for colloid contamination prior to use. We found that colloidal size distributions do not change in seawater samples stored for less than 24 h at 4°C. However, freezing and prolonged storage at 4°C can lead to alteration of colloidal size distributions (data not shown). All colloidal size distribution samples were run within 8 h of collection. Seawater for bulk CDOM absorbance measurements were treated the same as colloidal size samples but were filtered directly into acid-washed amber glass vials. The absorbance spectra of triplicate subsamples of room temperature bulk CDOM samples were obtained in the LWCC-2 within 2 h of seawater collection. Salinity was measured with a Fisher handheld refractometer (Fisher Scientific). Separate seawater samples were collected on a bidaily basis for Chl *a* over the duration of the study. Chl *a* was measured using the acidification method with a Turner Designs 10-AU fluorometer (calibrated with pure Chl *a*; Turner Designs), using Whatman GF/F filters, 7-min sonication, and 10-min acetone extraction.

**Culture experiments**—The production of colloidal material in algal cultures was investigated with the dinoflagellate *Alexandrium tamarense* and the diatom *Skeletonema menzelleri*. The clones were obtained from the Center for Culture of Marine Phytoplankton and originated in the Gulf of Maine. The cultures were grown in microwave-sterilized (Keller et al. 1988) artificial seawater media (Aquil; Morel et al. 1979; Price et al. 1989) amended to *f*/20 with Guillard's *f*/2 marine water enrichment solution (Sigma-Aldrich). The seawater media salinity and pH were equal to 32 and 8.1, respectively. Silica was added only to the diatom culture. All cultures were grown in acid-cleaned 50-mL glass tubes at 15°C under a 14:10 h light:dark cycle, using cool-white fluorescent bulbs at an intensity of  $0.86 \times 10^{16}$  quanta  $\text{cm}^{-2} \text{s}^{-1}$ .

We monitored culture growth on a bidaily basis for a total of 28 d using the *in vivo* chlorophyll fluorescence method of Brand and Guillard (1981). Fluorescence was measured on replicate cultures and on media blanks using a Turner Designs AU-10 fluorometer (Turner Designs).

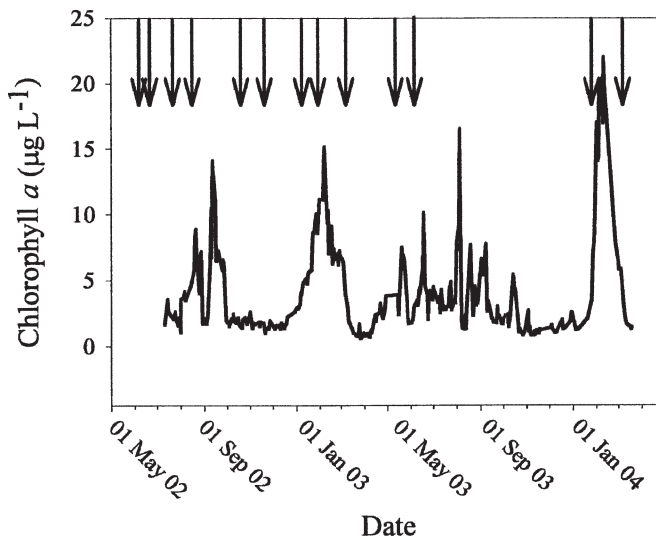


Fig. 2. Sampling dates and associated Chl *a* levels. The solid line represents Chl *a* and the arrows represent sampling time-points.

Colloidal size distributions were measured on cultures during log and senescent phases.

## Results

**Changes in colloidal size distribution and phytoplankton biomass**—We sampled colloidal size distributions in the range of 1–400 kDa (roughly equivalent to 1–40 nm diameter based on equivalent spherical diameter) in surface waters of the Damariscotta estuary on 13 dates over 22 months. During this time four distinct periods of elevated Chl *a* ( $>5 \mu\text{g L}^{-1}$ ) were observed and samples were collected as Chl *a* both increased and decreased, as well as during periods of low Chl *a* (Fig. 2).

Bulk seawater CDOM did not correlate with Chl *a* concentrations in surface waters of the Damariscotta estuary ( $r^2 = 0.079$ ,  $p = 0.590$ ) (data not shown). We also found no direct relationship between Chl *a* and total (i.e., 1–40 nm) colloidal absorbance ( $r^2$  values of 0.169,  $p = 0.418$ ; Fig. 3A); however, colloidal absorbance did increase significantly following periods of elevated phytoplankton biomass in the spring and summer of 2003 (Fig. 4A). Total colloidal absorbance was estimated by integration of colloidal size distribution peak areas and ranged from 120,000 to 393,000 response counts during the course of the study. The absorbance of small colloids ( $<18$  kDa; elution time 0–5 min) was positively correlated with Chl *a* ( $r^2 = 0.8187$ ,  $p = 0.013$ ) (Fig. 3B), and small colloids were primarily observed during periods of high phytoplankton biomass (Figs. 4B and 5). Although we found no overall correlation between Chl *a* and medium-sized colloids (18–150 kDa, elution time 5–25 min,  $r^2 = 0.230$ ,  $p = 0.336$ ; Fig. 3C), or with large colloids ( $>150$  kDa, elution time 25–40 min,  $r^2 = 0.138$ ; Fig. 3D), there were significant increases in medium and large colloidal absorbance *after* periods of elevated Chl *a* (Fig. 4C,D). There was no significant relationship between salinity and total colloidal absorbance ( $r^2 = 0.307$ ,

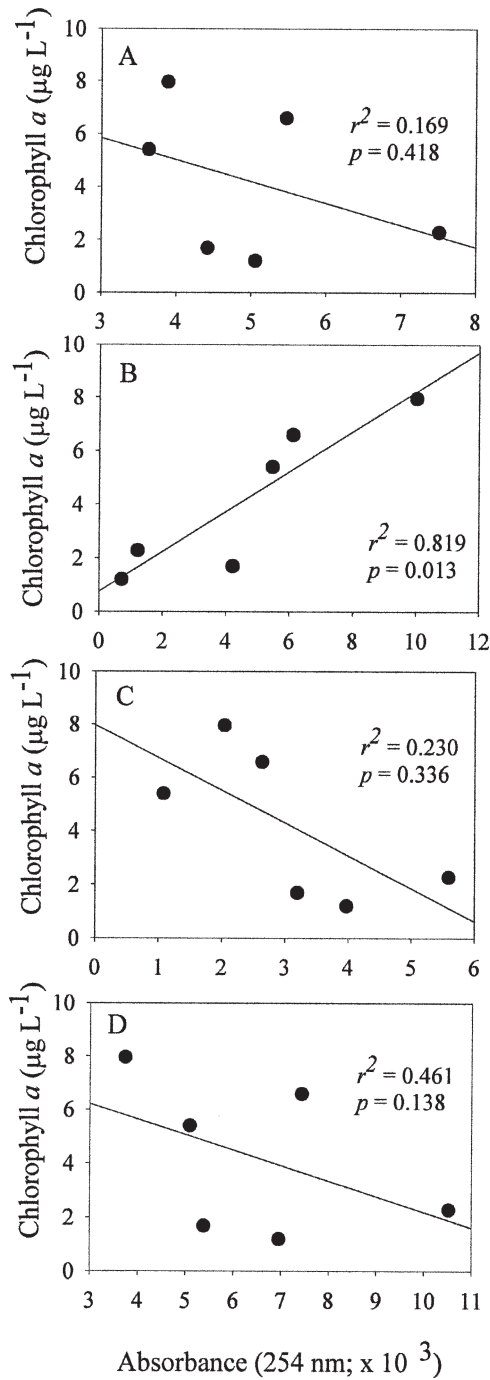


Fig. 3. The relationship between Chl *a* and absorbance (254 nm; in detector response units, integrated and normalized to elution time range) of (A) colloids sized 1–400 kDa, (B) small colloids (1–18 kDa), (C) medium colloids (18–150 kDa), and (D) large colloids (150–400 kDa).  $y$ -axes are identical; note the different scales on  $x$ -axes.

$p = 0.627$ ), nor between salinity and the absorbance of any of the size fractions ( $r^2$  and  $p$  values of 0.078 and 0.820, 0.191 and 0.712, and 0.159 and 0.739 for small, medium, and large colloids, respectively).

The bimodal colloidal size distribution observed in the Damariscotta estuary during periods of elevated

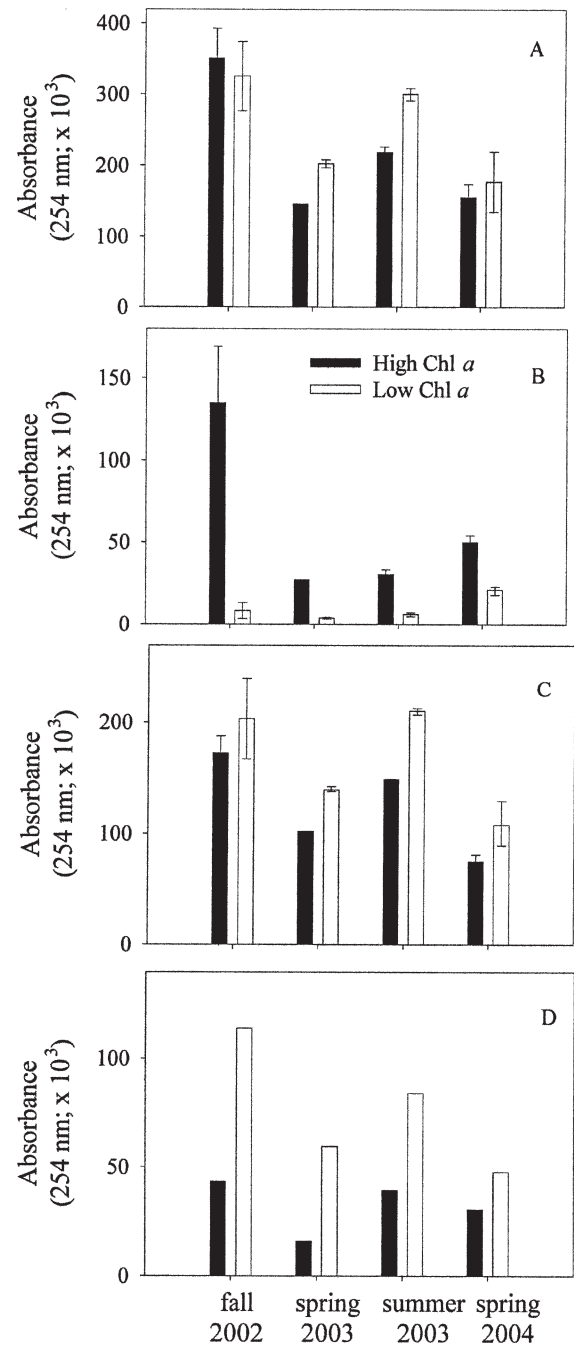


Fig. 4. Colloidal absorbance (in integrated detector response units) during high (>5 µg L<sup>-1</sup>) and low (<2.5 µg L<sup>-1</sup>) phytoplankton biomass over a 2-yr time period of colloids sized (A) 1–400 kDa, (B) <18 kDa, (C) 18–150 kDa, and (D) >150 kDa. Filled bars represent absorbance during high Chl *a*, and open bars represent absorbance during low Chl *a*. Error bars represent data range of at least two replicates, except for high Chl *a* spring 2003 and colloids >150 kDa where no error estimates are shown.  $x$ -axes are identical; note the different scales on  $y$ -axes.

Chl *a* (Fig. 5) was similar to that in senescent phytoplankton cultures (Fig. 6). Colloid absorbance was absent during exponential growth and was abundant during the senescence phase in growth experiments with both *A. tamarensis* and *S. menziesii* (Fig. 6). Chl *a* values during log

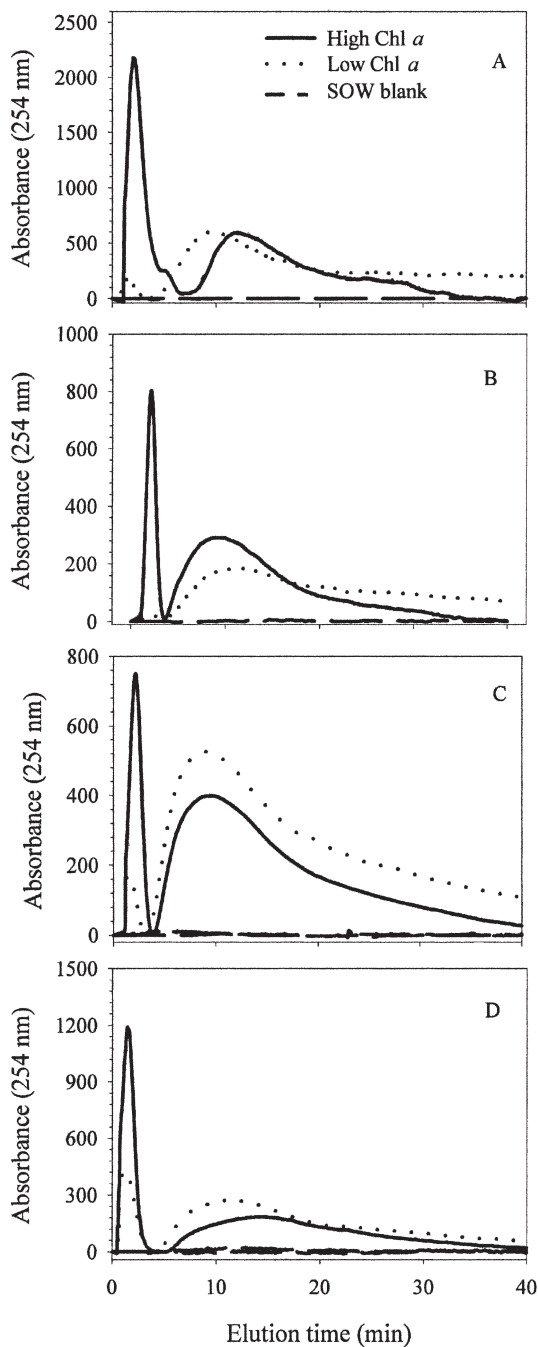


Fig. 5. Colloidal size distributions during high ( $>5 \mu\text{g L}^{-1}$ ) and low ( $<2.5 \mu\text{g L}^{-1}$ ) phytoplankton biomass over a 2-yr time period. (A) Fall 2002. (B) Spring 2003. (C) Summer 2003. (D) Spring 2004. These subplots correspond to bar groupings in Fig. 4. High Chl *a*, low Chl *a*, and seawater media blanks (SOW) are represented by solid, dotted, and dashed lines, respectively. Lines represent the mean of at least two replicate samples, except for high Chl *a* spring 2003 where no replicates were available. Replicate error is presented in Table 1. *x*-axes are identical; note the different scales on *y*-axes.

and senescence phases were  $0.8$  and  $1.3 \mu\text{g L}^{-1}$ , respectively, for *A. tamarensis* and  $4.1$  and  $3.9 \mu\text{g L}^{-1}$ , respectively, for *S. menzellerii*.

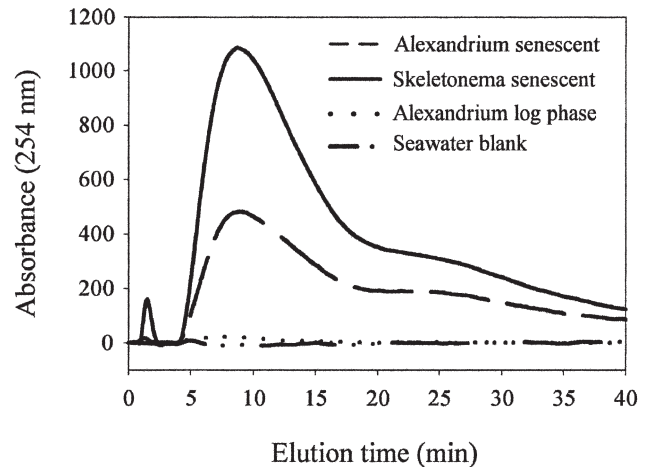


Fig. 6. Algal culture colloidal size distribution during log phase and senescence. Colloidal size distributions for *A. tamarensis* during log phase (dotted line) and senescence (dashed line), *S. menzellerii* during senescence (solid line), and seawater culture medium blank for log phase cultures (dash-dot line) are shown. Colloidal size distributions for *S. menzellerii* during log phase were indistinguishable from the *Alexandrium* log phase plot and the seawater blanks for log and senescent phase cultures. Lines represent the average of at least two replicates, and error estimates are shown in Table 1. Focus volumes of 5 mL were used for culture samples, whereas 50 mL focus volumes were used for field samples.

A direct relationship between peak area and amplitude (height) was observed for both small ( $r^2 = 0.964$ ,  $p = 4.91 \times 10^{-4}$ ) and medium-sized colloids ( $r^2 = 0.9852$ ,  $p = 8.30 \times 10^{-5}$ ). Similarly, peaks did not spread or encompass a greater range of elution time with increased area (data not shown). This result suggests that two primary size classes of colloids existed in the Damariscotta estuary and that the observed changes in absorbance do not reflect simple changes in the packaging of colloidal material. Distinct peaks were not observed for colloids greater than 150 kDa (Fig. 5).

Colloidal peak elution time is directly related to particle diameter (Fig. 1). The peak elution time of both the first and second peaks, corresponding to colloids  $<18$  kDa and 18–150 kDa, respectively, did not exhibit strong relationships with Chl *a* levels ( $r^2$  and  $p$  values of 0.501 and 0.116 for the first peak and 0.220 and 0.349 for the second). However, in each case the elution time of the  $<18$  kDa colloidal fraction decreased significantly following periods of elevated Chl *a* (data not shown), indicating that the dominant size class of colloids became smaller. The second colloidal peak (18–150 kDa) exhibited a reduced elution time on two sampling occasions, the fall of 2002 and spring of 2004.

*Changes in magnitude of CDOM absorption*—The CDOM absorbance of filtered seawater ( $0.2 \mu\text{m}$ ) was measured on seven dates between November 2002 and March 2004. This sampling period coincided with three periods of elevated phytoplankton biomass. The total range of CDOM absorption at 400 nm was  $0.360$  to  $0.941 \text{ m}^{-1}$ ,

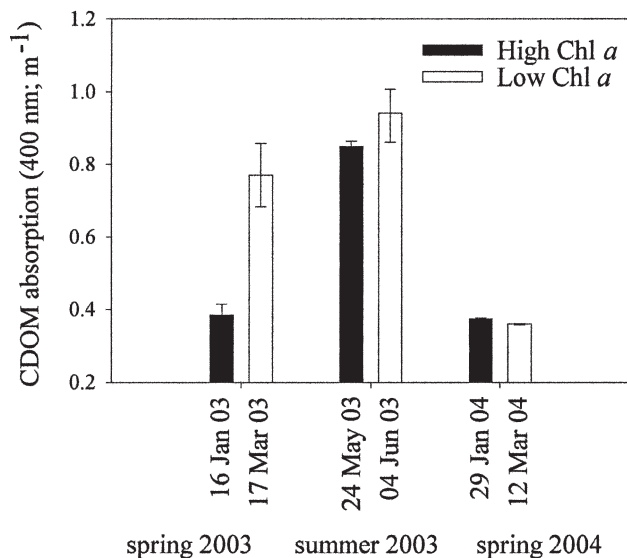


Fig. 7. Variations in CDOM absorption of bulk filtered seawater during high ( $>5 \mu\text{g L}^{-1}$ ) and low ( $<2.5 \mu\text{g L}^{-1}$ ) phytoplankton biomass. Filled bars represent high Chl *a*, and open bars represent low Chl *a*. Error bars represent the range of three replicates.

and absorption was significantly higher between March and June of 2003 than at any other time during the course of the study (Fig. 7). CDOM absorbance was high during both high and low Chl *a* periods during this time interval. We found no significant correlation between CDOM absorption and Chl *a* ( $r^2 = 0.079$ ,  $p = 0.590$ ); however, there was a positive correlation between CDOM absorption and total colloidal absorbance ( $r^2 = 0.772$ ,  $p = 0.021$ ; Fig. 8A), as well as with absorbance of the 18–150 kDa sized colloids ( $r^2 = 0.813$ ,  $p = 0.014$ ; Fig. 8C). CDOM absorption was not significantly correlated with the absorbance of the smaller (1–18 kDa) colloids ( $r^2 = 0.356$ ,  $p = 0.212$ ; Fig. 8B) or those sized 150–400 kDa ( $r^2 = 0.525$ ,  $p = 0.103$ ; Fig. 8D). There also was no correlation between salinity and CDOM absorption ( $r^2 = 0.222$ ,  $p = 0.688$ ).

*Changes in CDOM spectral slope of bulk filtered seawater and colloidal size fractions*—The spectral slopes,  $S$  ( $\text{nm}^{-1}$ ), of filtered ( $0.2 \mu\text{m}$ ) seawater samples were determined on six dates between January 2003 and March 2004. The range in  $S$  was  $0.0163$  to  $0.0183 \text{ nm}^{-1}$ , with a significantly higher slope ( $0.0249 \text{ nm}^{-1}$ ) measured on 04 June 2003 (Fig. 9). The spectral slope of CDOM was not directly related to Chl *a* concentration ( $r^2 = 0.111$ ,  $p = 0.519$ ); however, a pattern of increasing slope following periods of elevated Chl *a* was evident in the summer of 2003 and spring of 2004 (Fig. 9). There was no significant correlation between salinity and CDOM spectral slope ( $r^2 = 0.040$ ,  $p = 0.872$ ).

Multiple spectral slopes were determined for colloids eluting from the flow FFF in each of the size classes studied; 1, 2, and 3 min ( $<18 \text{ kDa}$  size fraction); 7, 10, 13, 20, and 24 min (18–150 kDa size fraction); and 28, 32, and 36 min ( $>150 \text{ kDa}$  size fraction). The spectral slopes of

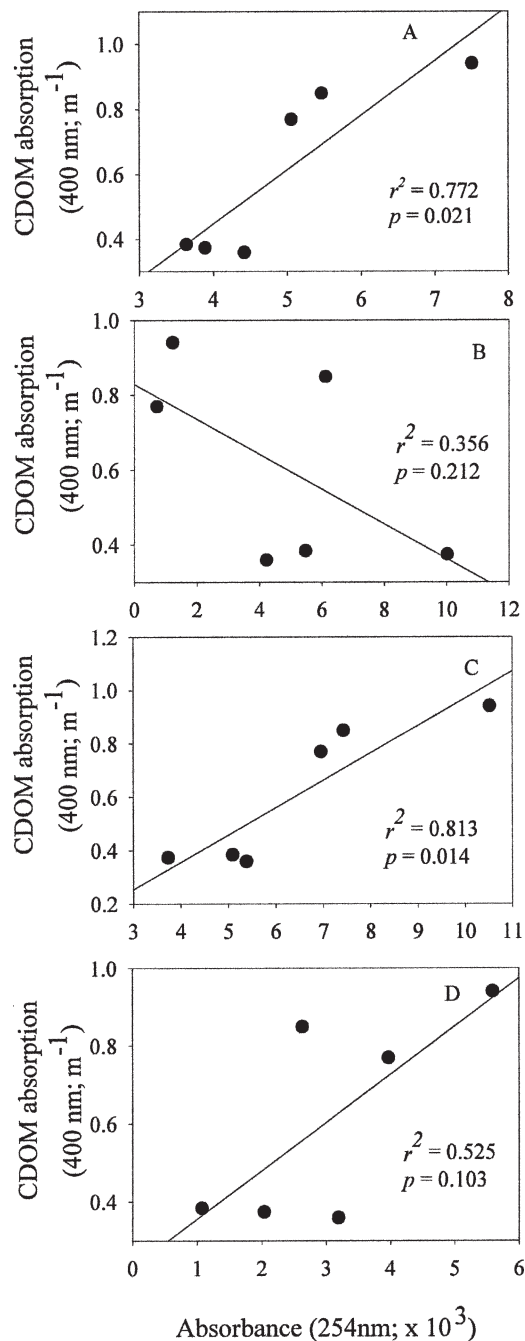


Fig. 8. CDOM absorption (400 nm) of bulk filtered seawater vs. absorbance (254 nm) of (A) colloids sized 1–400 kDa, (B) small colloids (1–18 kDa), (C) medium colloids (18–150 kDa), and (D) large colloids (150–400 kDa). Note the different x- and y-axes.

colloidal fractions varied greatly within a single sample and even within a single size class (Fig. 10). For example, on 24 May 2003 the range of spectral slopes observed within size classes were  $0.0114$ – $0.0162 \text{ nm}^{-1}$  ( $<18 \text{ kDa}$ ),  $0.0134$ – $0.0160 \text{ nm}^{-1}$  (18–150 kDa), and  $0.0115$ – $0.013 \text{ nm}^{-1}$  (150–400 kDa; Fig. 10C).

The spectral slope of material eluting at 1 min (i.e., the fraction closest in size to truly soluble CDOM) was greater

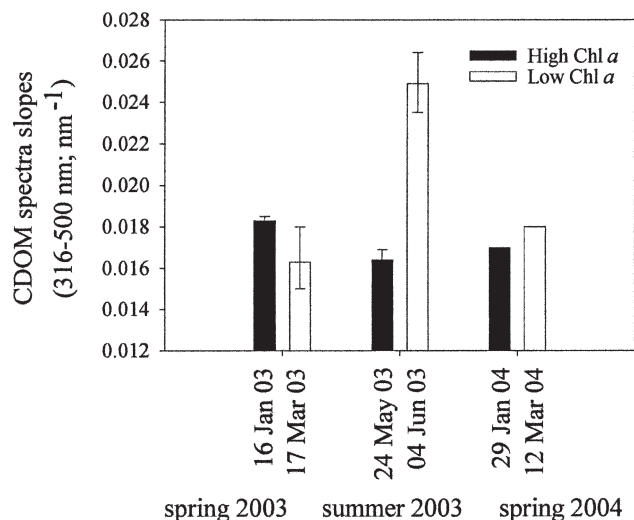


Fig. 9. Variations in the spectral slope of CDOM in bulk filtered seawater during high ( $>5 \mu\text{g L}^{-1}$ ) and low ( $<2.5 \mu\text{g L}^{-1}$ ) phytoplankton biomass. Filled bars represent high Chl *a* and open bars represent low Chl *a*. Error bars represent the range of three replicates.

than or equal to that of colloids eluting at 2 and 3 min in all samples. The greatest range in slopes of colloidal fractions  $<18$  kDa was evident on 16 January 2003 (0.0094–0.0153  $\text{nm}^{-1}$ ) (unfortunately no replicates were measured for this date). The differences in the spectral slope among  $>18$  kDa colloid fractions were more pronounced during periods of high Chl *a* than during periods of low Chl *a* (Fig. 10). The slope of filtered seawater was greater than or equal to that of the colloidal fractions in all of the samples (Fig. 10).

## Discussion

In areas of low freshwater input, phytoplankton are believed to be the primary source of CDOM. However, there is no clear positive correlation between Chl *a* and CDOM absorption in coastal (Boss et al. 2001) or open ocean (Bricaud et al. 1981; Nelson et al. 1998) environments. We also found no correlation between Chl *a* and CDOM absorption ( $r^2 = 0.079$ ,  $p = 0.590$ ) in our data, but CDOM absorption did correlate positively with the absorbance of  $\sim 1$ –40 nm sized colloids ( $r^2 = 0.772$ ,  $p = 0.021$ ). Additionally, both CDOM absorption (400 nm), and total colloidal absorbance (254 nm) increased following the periods of elevated phytoplankton biomass in spring and summer of 2003. We found no significant correlation between the observed small variations in salinity and colloidal absorbance, CDOM absorption (400 nm) or spectral slope, indicating that the changes we observed were not related to riverine inputs. These findings suggest that phytoplankton are a direct source of colloidal material and that this material contributes significantly to the overall optical signature of coastal seawater.

*Colloidal dynamics in the Damariscotta estuary*—Colloid size distribution: Two characteristic colloidal size distribu-

tions were observed throughout the course of this study: one bimodal distribution with peaks centered at 2 and 10 min elution times, and one with only a single broad peak centered at 10 min elution time (Fig. 5). The peak elution times observed correspond to approximate molecular weights of 2 and 45 kDa, respectively, based on our calibration with polystyrene sulfonate molecular weight standards. We chose to separate the colloids into three size classes based on the observed size distributions. In the discussion that follows, colloids  $<18$ , 18–150, and 150–400 kDa refer to those eluting from the flow FFF channel at  $\sim 0$ –5, 5–25, and 25–40 min, respectively. We would like to point out that the colloidal size distributions observed here are comparable to those reported in Boehme and Wells (2006) despite the use of slightly different size class divisions. We are cautious in reporting colloidal size distributions in terms of molecular weight because errors may occur if the physical (i.e., shape) and chemical behavior of natural colloids within the flow FFF channel differs from that of the molecular weight standards.

The size distribution of marine particles is largely influenced by physical interactions, such as the coagulation of small particles and the breakup of large aggregates (McCave 1984; Jackson 1995). The size spectra of oceanic particles, including colloids, typically fit a power function model in which particle numbers increase with decreasing size (Johnson and Kepkay 1992; Wells and Goldberg 1994). Some earlier studies investigating marine colloids using flow FFF have reported primarily monodisperse colloidal size distributions with a peak in absorbance (as a proxy for abundance) at  $\sim 1$ –2 kDa (Lyven et al. 1997; Zanardi-Lamardo et al. 2001, 2002). However, other studies report distinct peaks in abundance of certain colloidal size classes (Yamasaki et al. 1998; Vaillancourt and Balch 2000). Vaillancourt and Balch (2000) observed distinct flow FFF peaks in colloidal absorbance at 4, 20, and 100 nm, while Yamasaki et al. (1998) used ultrafiltration and found a high abundance of colloids 600–700 nm in highly productive coastal waters and size distributions closer to the power function model in less productive deep and offshore waters.

Unfortunately, it currently is difficult to critically compare colloidal size distributions among these and other studies because of the different methods used for colloid isolation and concentration. Comparisons are difficult even among flow FFF studies because of differences in instrument operating conditions (Fløge unpubl. data). For example, earlier studies have used carrier solutions composed of tris(hydroxymethyl)aminomethane (Trisma, Aldrich) in deionized water (pH 8, ionic strength  $0.08 \text{ mol L}^{-1}$ ) and added surfactants to minimize the adsorption of natural colloids in the system (Lyven et al. 1997; Zanardi-Lamardo et al. 2001, 2002). However, we found colloid adsorption to be minimal when seawater or synthetic seawater carrier solutions are used. Moreover, a phosphate buffer carrier solution dramatically changed our colloid size distribution, sharply increasing the abundance of smaller colloids eluting at 2 min while eliminating the larger colloidal material eluting at 10 min. We speculate that high concentrations of buffers and ionic surfactants have the potential to disrupt the internal

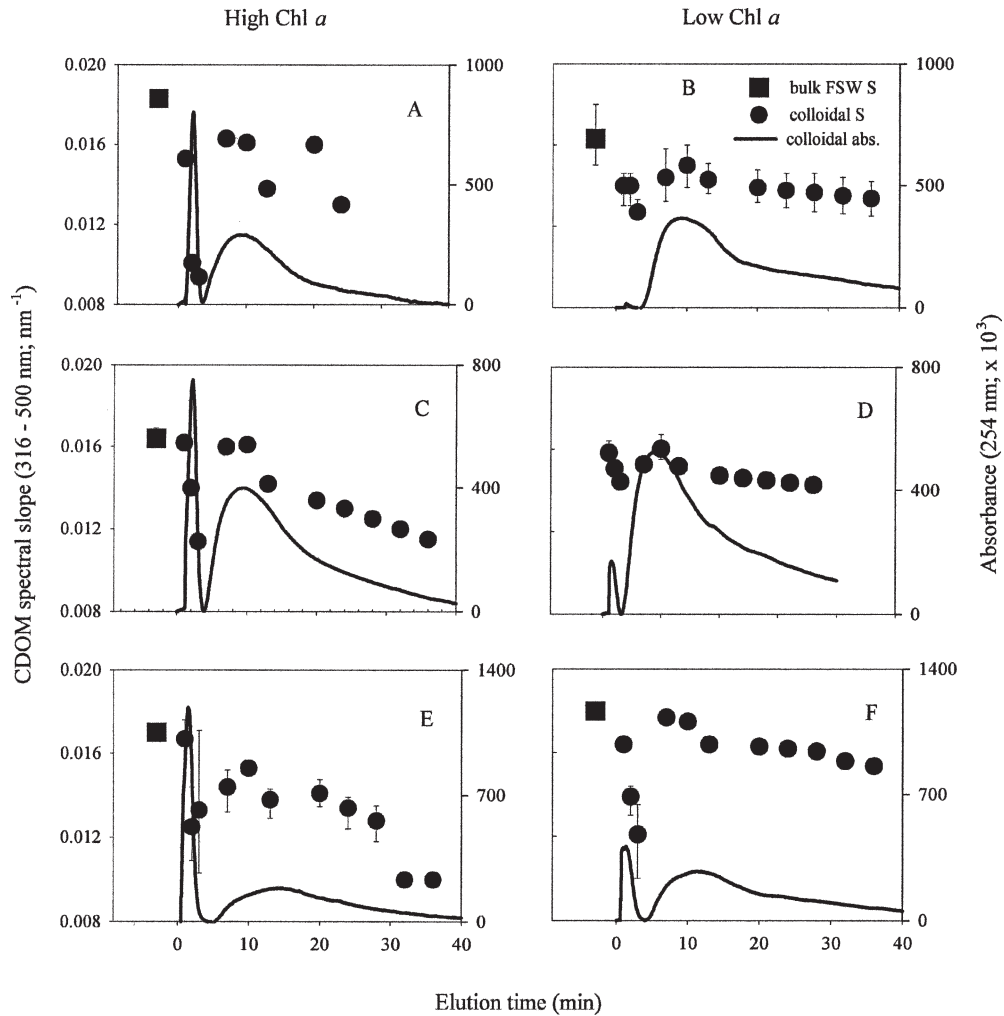


Fig. 10. Variations in CDOM absorption spectra slopes with colloid size and colloidal size distribution. (A) 16 Jan 03. (B) 17 Mar 03. (C) 24 May 03. (D) 04 Jun 03. (E) 29 Jan 04. (F) 12 Mar 04. The solid line represents the average colloidal size distribution as measured by flow FFF UV-Vis detector. The filled circles represent the spectral slope of colloids eluting from the flow FFF channel at the specified time point. Colloids eluting from the flow FFF channel between 1 and 5 min are <18 kDa, between 5 and 25 min are sized 18–150 kDa, and 25–40 min are 150–400 kDa. Filled squares represent the spectral slope of bulk filtered seawater. All error bars represent the slope range on two replicate samples and are smaller than the symbol size where not evident (except for the bulk sample from 12 Mar 04 and the size-fractionated sample from 16 Jan 03 due to insufficient sample numbers). Spectral slope of bulk seawater was off scale at  $0.025 \text{ nm}^{-1}$  on 04 Jun 03 with a range of  $0.0235\text{--}0.0264 \text{ nm}^{-1}$ . All panels have identical  $x$ - and left  $y$ -axes; note different right  $y$ -axes.

structure of marine colloids by decreasing  $\text{Ca}^{2+}$  activity (Chin et al. 1998). We suggest that using a carrier solution as similar to natural seawater as possible will be important for gaining realistic insights into the size distribution of marine colloidal matter.

Our use of flow FFF for the study of natural colloids requires two basic assumptions. First that absolute colloidal mass is proportional to the magnitude of UV absorption at 254 nm. However, chromophores may not be uniformly distributed across the colloidal size range under investigation, thereby leading to inaccurate representations of colloidal size distributions and mass abundance. For example, colloidal size fractions with a high spectral slope

may be overrepresented in terms of total colloidal absorbance because these materials preferentially absorb at lower wavelengths. For this reason these data presented here and the discussion below focus on relative changes in colloidal CDOM absorbance and size distribution over time rather than absolute colloidal mass. Second, there is a concern that absorbance of colloidal CDOM at 254 nm is not proportional to the absorbance of bulk filtered seawater CDOM (absorbing at 400–700 nm). However, preliminary comparisons of fractograms measured at 254 nm and wavelengths above 350 nm showed qualitatively similar size distributions at high CDOM absorbance. Unfortunately, the detector sensitivity was

not sufficient to routinely use these higher wavelengths in our flow FFF study. We assume here that this qualitative agreement also holds for lower bulk CDOM absorbances, but this issue remains an area for future research.

**Seasonal changes in colloid abundance:** There have been only a few studies examining the relationship between Chl *a* and colloid abundance in the natural environment. Strong positive correlations between Chl *a* and the abundance of colloids sized 400–1,000 nm have been found in the Pacific Ocean (Koike et al. 1990; Yamasaki et al. 1998), and covariance between Chl *a* and the abundance of small colloids (5–200 nm) with depth was observed by Wells and Goldberg (1994) in the North Atlantic and Southern Oceans. These data suggest that phytoplankton are a primary source of marine colloids. Indeed, the direct production of high molecular weight (>1 kDa) organic matter by phytoplankton has been well documented (e.g., Hellebust 1965; Biddanda and Benner 1997). Other biological sources of marine colloids likely include heterotrophic bacterial activity (Biddanda 1988; Amon and Benner 1996), release by grazers (via sloppy feeding, egestion, or excretion) (Eppley et al. 1981; Jumars et al. 1989), release of metabolic wastes by protozoans (Koike et al. 1990), and viral lysis of algae or bacteria (Proctor and Fuhrman 1991).

We observed the production of colloids in culture experiments with both the centric diatom *S. menzellii* and the dinoflagellate *A. tamarensis* (Fig. 6). Colloid abundance in these cultures was greatest during the senescence phase and thus might be derived directly from leaky phytoplankton cells and indirectly through the aggregation of truly dissolved organic matter and increased bacterial activity. A very similar pattern of colloid production was observed in cultures of the pennate diatom of the genus *Pseudonitzschia* (Wells 2004). While these monoclonal cultures would not be representative of colloid production dynamics in natural systems, it is noteworthy that the colloidal size distributions in these cultures were similar to those observed in coastal waters of the Damariscotta estuary during periods of high Chl *a* (>5  $\mu\text{g L}^{-1}$ ).

Although the sampling frequency in this study was too coarse to measure the direct effect of phytoplankton bloom progression on colloidal abundance, there were clear patterns of changing colloidal absorbance across seasons (Fig. 4). A more than threefold variation in total colloidal absorbance was observed, with significantly higher absorbance occurring in summer and fall than in spring (Fig. 4). Bulk CDOM absorption also was found to be higher in summer than in spring (Fig. 7). These seasonal variations may reflect the differences in the background phytoplankton abundance, which is at a minimum preceding the spring bloom. The lowest colloidal absorbance observed in our study (spring 2003) occurred following the longest stretch of low Chl *a* levels observed (<2  $\mu\text{g L}^{-1}$  between October and December 2002). Given an expected lower rate of colloid production by phytoplankton during winter months, colloid removal processes, such as aggregation (Baskaran et al. 1992; Moran and Buesseler 1992; Wells and Goldberg 1993), grazing (Tranvik et al. 1993), and enzyme hydrolysis (Nagata and Kirchman 1996), may

dominate to create low colloid abundance immediately preceding the spring bloom. A similar pattern of increased CDOM absorption following spring phytoplankton blooms was found over a 4-yr period in the Sargasso Sea by Nelson et al. (1998, 2004). Multiyear and higher resolution sampling will be necessary to verify this apparent trend.

We found a direct relationship between Chl *a* and the absorbance of colloids sized 1–18 kDa ( $r^2 = 0.819$ ,  $p = 0.013$ ; Fig. 3B) in the Damariscotta estuary. While we did not find significant correlation between Chl *a* and total colloidal absorbance (Fig. 3A), nor between Chl *a* and the absorbance of larger colloids (18–150 kDa, 150–400 kDa; Figs. 3C and D), we did observe a general pattern of increasing colloidal absorbance following periods of elevated phytoplankton biomass (Fig. 4A, C, and D). Colloids <18 kDa were virtually absent during periods of low Chl *a* ( $n = 6$ ; data not shown), showed high absorbance during periods of high phytoplankton biomass, and exhibited decreases in absorbance concomitant with decreases in Chl *a* concentrations. Based on this measure, small colloids appeared to be the most dynamic fraction within the size range investigated here. The apparently direct relationship with Chl *a* and their rapid appearance and subsequent disappearance (data not shown) suggests that these colloids may be directly produced by phytoplankton and comprise highly labile organic matter. Indeed, fluorescence analyses of colloids <18 kDa revealed a protein-like signature, whereas larger colloids have a humic-like fluorescence signature (Boehme and Wells 2006). The increase in colloids >18 kDa with bloom progression suggests that secondary production such as cell leakage, lysis, or grazing may be important mechanisms of formation for this size class. Aggregation of small colloids (e.g., <18 kDa) also has been suggested to be a dominant mechanism for the formation of larger colloidal phases (Wells and Goldberg 1993; Chin et al. 1998). Although we cannot assess this possibility from these data, the year-round presence of colloids >18 kDa suggests that they may be less chemically labile than their smaller counterparts. However, this apparent persistence of larger colloids also might obscure highly dynamic production and removal processes that remain largely in balance year-round.

Advection of water masses over both short (e.g., tidal cycles) and longer time scales is always an important consideration when conducting work in dynamic environments such as estuaries. We found no significant change in colloidal size distributions or CDOM optical characteristics over tidal cycles ( $n = 3$  tidal cycles over multiple seasons), as well as no significant correlations between salinity and colloidal absorbance, CDOM absorption (400 nm), or spectral slope. These data indicate that water mass advection did not play a large role in determining the optical characteristics of both bulk filtered seawater and colloidal material at our study site.

*Variations in CDOM signature*—CDOM spectral slope of bulk filtered seawater: The slope, *S*, of CDOM absorption spectra is believed to differ according to CDOM source and to change with biological and chemical

transformations of the source material (Nelson and Siegel 2002, and references within). Values of  $S$  reported in the literature range from  $0.010 \text{ nm}^{-1}$  to greater than  $0.025 \text{ nm}^{-1}$ , with higher values typically found in open ocean environments (Nelson and Siegel 2002, and references within). However, it is difficult to compare results among studies because of differences in the wavelength ranges and curve fitting techniques used to calculate  $S$  (Nelson and Siegel 2002, and references within; Twardowski et al. 2004). We observed bulk CDOM spectral slopes between  $0.0163$  and  $0.0183 \text{ nm}^{-1}$ , with an exceptional value of  $0.0249 \text{ nm}^{-1}$  measured on 04 June 2003 (Fig. 9). These values suggest that our study area was dominated by waters having coastal type CDOM characteristics, with the exception of a possible intrusion event of offshore water in early June 2003.

Although our sampling frequency does not allow close scrutiny of changes in  $S$  during phytoplankton blooms, CDOM spectral slope values increased significantly following periods of increased Chl  $a$  in the summer of 2003 and spring of 2004 (but not spring 2003; Fig. 9). This finding agrees with patterns found in the Sargasso Sea by Nelson et al. (2004). Specifically, Nelson and coworkers observed increases in CDOM spectral slope in subsurface waters throughout summer months, which they attributed to microbial processing (i.e., removal) of phytoplankton-derived CDOM precursors. However, removal of CDOM via photobleaching (Mopper and Kieber 2002, and references within) and increased colloid aggregation associated with phytoplankton bloom progression (Niven et al. 1995) could also cause variations in CDOM spectral slope. Thus, it is unclear whether changes we observed in  $S$  were due predominantly to biological, photochemical, or aggregation processes.

Colloidal particles have been implicated as a major source of particulate backscattering in seawater (Stramski et al. 2004, and references within). This scattering is of concern here because it could contribute significantly to bulk CDOM absorption signals, particularly those measured with a liquid core waveguide, and thus potentially affect spectral slope values. However, we found no significant differences in absorption of molecular weight standards sized 14, 45, and 150 kDa (Fløge unpubl. data) indicating that scattering by colloids in the size range of 14–150 kDa did not affect our absorption data. Similarly, we found no significant correlation between colloids <18 kDa and CDOM absorption ( $r^2 = 0.356$ ,  $p = 0.212$ ), indicating that colloid scattering effects by very small colloids were not significant in these CDOM absorption measurements.

Variations in  $S$  with molecular weight: The continuum of size separation offered by flow FFF was used to assess variations in  $S$  as a function of colloidal size. We observed large variations in  $S$  for colloids in the 1–400 kDa size range (e.g.,  $0.0094$ – $0.0153 \text{ nm}^{-1}$  on 16 January 2003) (Fig. 10). Colloids greater than 18 kDa displayed general trends of decreasing  $S$  with increasing molecular weight (Fig. 10), as is commonly observed for humic materials (Hayase and Tsubota 1985; Carder et al. 1989). As noted above, spectrofluorometric analyses of the colloidal material in this study revealed humic-like signatures in the

>18 kDa size fraction and protein-like signatures in the <18 kDa colloidal fraction (Boehme and Wells 2006). Thus, compositional differences in small and large colloidal material may account for some of the spectral slope variability. The relationship between  $S$  and molecular weight has been investigated by Mopper et al. (1996) and Yacobi et al. (2003) using ultrafiltration. Although the findings by Yacobi et al. (2003) support the simple inverse relationship between molecular weight and  $S$ , Mopper et al. (1996) suggest that the relationship between  $S$  and size is variable. Mopper et al. (1996) report that the average spectral slope of colloidal material was significantly lower than the bulk CDOM slope in highly productive coastal waters, whereas the opposite was found in deep non-productive oceanic waters. Our data also show the spectral slope of colloidal material was lower than bulk CDOM in highly productive (high Chl  $a$ ) waters. These data indicate that bulk and colloidal CDOM differ in their chromophoric composition, and thus that phytoplankton production will influence CDOM spectral characteristics. By inference, truly soluble (<1 kDa) CDOM might be expected to have had higher spectral slopes than the colloidal fraction measured here, assuming that CDOM spectral slopes arise from the linear addition of spectra from many independent chromophores. However, this assumption recently has been called into question (Del Vecchio and Blough 2004).

There presently is little known about the role of colloidal material in ocean optics, even though a major fraction of dissolved organic carbon exists in colloidal phases. Although these substances often are termed high molecular weight matter, this label is conceptually inadequate because it leads one to overlook interfacial processes that may dominate loss mechanisms for CDOM. This study shows there are changes in colloid abundance and size distributions, and CDOM absorption and spectral slope associated with phytoplankton biomass. Colloidal abundance was positively correlated with CDOM absorption (400 nm), whereas the spectral slope of colloidal size fractions spanned a range as large as that observed between offshore and nearshore waters. That, along with observed dynamics in the abundance of different colloidal size fractions, suggests that the marine CDOM matrix is not uniform in composition but one in which its subcomponents exist physically distinct from one another. Ascertaining and quantifying the physical, biological, and chemical processes acting on these distinct packages will provide the basis for gaining predictive insights to the behavior of marine CDOM.

## References

- AMON, R. M. W., AND R. BENNER. 1996. Bacterial utilization of different size classes of dissolved organic matter. *Limnol. Oceanogr.* **41**: 41–51.
- BAINES, S. B., AND M. L. PACE. 1991. The production of dissolved organic matter by phytoplankton and its importance to bacteria: Patterns across marine and freshwater systems. *Limnol. Oceanogr.* **36**: 1078–1090.
- BASKARAN, M., P. H. SANTSCHI, G. BENOIT, AND B. D. HONEYMAN. 1992. Scavenging of thorium isotopes by colloids in seawater of the Gulf of Mexico. *Geochim. Cosmochim. Acta* **56**: 3375–3388.

- BECKETT, R., AND B. T. HART. 1993. Use of field-flow fractionation techniques to characterize aquatic particles, colloids and macromolecules. *In* J. Buffle and H. P. v. Leeuwen [eds.], Environmental particles. Lewis.
- BELZ, M., P. DRESS, A. SUKHITSKIY, AND S. LIU. 1999. Linearity and effective optical pathlength of liquid waveguide capillary cells. *SPIE* **3856**: 271–281.
- BENNER, R., J. D. PAKULSKI, M. MCCARTHY, J. I. HEDGES, AND P. G. HATCHER. 1992. Bulk chemical characteristics of dissolved organic matter in the ocean. *Science* **255**: 1561–1564.
- BIDDANDA, B. A. 1988. Microbial aggregation and egradation of phytoplankton-derived detritus in seawater. II. Microbial metabolism. *Mar. Ecol. Prog. Ser.* **42**: 89–95.
- , AND R. BENNER. 1997. Carbon, nitrogen, and carbohydrate fluxes during the production of particulate and dissolved organic matter by marine phytoplankton. *Limnol. Oceanogr.* **42**: 506–518.
- BLOUGH, N. V., AND R. DEL VECCHIO. 2002. Chromophoric DOM in the coastal environment, p. 509–546. *In* D. A. Hansell and C. A. Carlson [eds.], Biogeochemistry of marine dissolved organic matter. Academic.
- , AND R. G. ZEPP. 1995. Reactive oxygen species in natural waters, p. 280–333. *In* C. S. Foote, et al. [eds.], Active oxygen: Reactive oxygen species in chemistry. Chapman and Hall.
- BOEHME, J., AND M. WELLS. 2006. Fluorescence variability of marine and terrestrial colloids: Examining size fractions of chromophoric dissolved organic matter in the Damariscotta River estuary. *Mar. Chem.* **101**: 95–103.
- BOSS, E., W. S. PEGAU, J. R. V. ZANEVELD, AND A. H. BARNARD. 2001. Spatial and temporal variability of absorption by dissolved material at a continental shelf. *J. Geophys. Res.* **106**: 9499–9507.
- BRAND, L. E., AND R. R. L. GUILLARD. 1981. A method for the rapid and precise determination of acclimated phytoplankton reproduction rates. *J. Plankton Res.* **3**: 193–201.
- BRICAUD, A., A. MOREL, AND L. PRIEUR. 1981. Absorption by dissolved organic matter of the sea (yellow substance) in the UV and visible domains. *Limnol. Oceanogr.* **26**: 43–53.
- BUESSELER, AND OTHERS. 1996. An intercomparison of cross-flow techniques for sampling marine colloids: Overview and organic carbon results. *Mar. Chem.* **51**: 1–31.
- CARDER, K. L., R. G. STEWARD, G. R. HARVEY, AND P. B. ORTNER. 1989. Marine humic and fulvic acids: Their effects on remote sensing of chlorophyll. *Limnol. Oceanogr.* **34**: 68–81.
- CHIN, W. C., M. V. ORELLANA, AND P. VERDUGO. 1998. Spontaneous assembly of marine dissolved organic matter into polymer gels. *Nature* **391**: 568–572.
- DEL VECCHIO, R., AND N. V. BLOUGH. 2004. On the origin of the optical properties of humic substances. *Environ. Sci. Technol.* **38**: 3885–3891.
- EPPLEY, R. W., S. G. HERRIGAN, J. A. FUHRMAN, E. R. BROOKS, C. C. PRICE, AND K. SELLNER. 1981. Origins of dissolved organic matter in southern California coastal waters: Experiments on the role of zooplankton. *Mar. Ecol. Prog. Ser.* **6**: 149–159.
- GIDDINGS, J. C. 1993. Field-flow fractionation: Analysis of macromolecular, colloidal and particulate materials. *Science* **260**: 1456–1465.
- , M. N. MYERS, F. J. YANG, AND L. K. SMITH. 1976. Mass analysis of particles and macromolecules by field-flow fractionation, p. 381–398. *In* M. Kerker [ed.], Colloid and interface science. Academic.
- , F. J. YANG, AND M. N. MYERS. 1977. Flow field-flow fractionation: New method for separating, purifying and characterizing the diffusivity of viruses. *J. Virol.* **21**: 131–138.
- GUO, L., C. H. COLEMAN, AND P. H. SANTSCHI. 1994. The distribution of colloidal and dissolved organic carbon in the Gulf of Mexico. *Mar. Chem.* **45**: 105–119.
- HARRIS, J. E. 1977. Characterization of suspended matter in the Gulf of Mexico—II. Particle size analysis of suspended matter from deep water. *Deep Sea Res.* **24**: 1055–1061.
- HASSELHOV, M., B. LYVEN, C. HARALDSSON, AND D. TURNER. 1996. A flow field-flow fractionation system for size fractionation of dissolved organic matter in seawater and freshwater using on-channel preconcentration. 6th International Symposium of FFFF, Ferra, Italy.
- HAYASE, K., AND H. TSUBOTA. 1985. Sedimentary humic acid and fulvic acid as fluorescent organic materials. *Geochim. Cosmochim. Acta* **49**: 159–163.
- HELLEBUST, J. A. 1965. Excretion of some organic compounds by marine phytoplankton. *Limnol. Oceanogr.* **10**: 192–206.
- HOCHMAN, H., F. E. MULLER-KARGER, AND J. J. WALSH. 1994. Interpretation of the color signature of the Orinoco River plume. *J. Geophys. Res.* **99**: 7443–7455.
- JACKSON, G. A. 1995. Comparing observed changes in particle size spectra with those predicted using coagulation theory. *Deep-Sea Res. II* **42**: 159–184.
- JERLOV, N. G. 1976. Marine optics, 2nd ed. Elsevier.
- JOHNSON, B. D., AND P. E. KEPKAY. 1992. Colloid transport and bacterial utilization of oceanic DOC. *Deep-Sea Res.* **39**: 855–869.
- JUMARS, P. A., D. L. PENRY, J. A. BAROSS, M. J. PERRY, AND B. W. FROST. 1989. Closing the microbial loop: Dissolved carbon pathway to heterotrophic bacteria from incomplete ingestion, digestion and absorption in animals. *Deep-Sea Res.* **36**: 483–495.
- KELLER, M. D., W. K. BELLOWS, AND R. R. L. GUILLARD. 1988. Microwave treatment for sterilization of phytoplankton culture media. *J. Exp. Mar. Biol. Ecol.* **117**: 279–283.
- KIEBER, D. J., J. A. MCDANIEL, AND K. MOPPER. 1989. Photochemical source of biological substrates in seawater: Implications for geochemical carbon cycling. *Nature* **341**: 637–639.
- KOIKE, I., S. HARA, K. TERAUCHI, AND K. KOGUE. 1990. Role of sub-micron particles in the ocean. *Nature* **345**: 242–244.
- LONGHURST, A. R., AND OTHERS. 1992. Sub-micron particles in northwest Atlantic shelf water. *Deep-Sea Res.* **39**: 1–7.
- LYVEN, B., M. HASSELHOV, C. HARALDSSON, AND D. R. TURNER. 1997. Optimisation of on-channel preconcentration in flow field-flow fractionation for the determination of size distributions of low molecular weight colloidal material in natural waters. *Anal. Chim. Acta* **357**: 187–196.
- MCCAVE, I. N. 1984. Size spectra and aggregation of suspended particles in the deep ocean. *Deep-Sea Res.* **31**: 329–352.
- MILLER, W. L. 1994. Recent advances in the photochemistry of natural dissolved organic matter, p. 111–127. *In* G. R. Helz, et al. [eds.], Aquatic and surface photochemistry. Lewis.
- MOPPER, K., Z. FENG, S. BENTJEN, AND R. F. CHEN. 1996. Effects of cross-flow filtration on the absorption and fluorescence properties of seawater. *Mar. Chem.* **55**: 53–74.
- , AND D. J. KIEBER. 2002. Chromophoric DOM in the open ocean, p. 547–578. *In* D. A. Hansell and C. A. Carlson [eds.], Biogeochemistry of marine dissolved organic matter. Academic.
- MORAN, S. B., AND K. O. BUESSELER. 1992. Short residence times of colloids in the upper ocean estimates from <sup>238</sup>U–<sup>234</sup>Th disequilibria. *Nature* **359**: 221–223.
- MOREL, F. M. M., J. G. REUTER, D. M. ANDERSON, AND R. R. L. GUILLARD. 1979. Aquil: A chemically defined phytoplankton culture medium for trace metal studies. *J. Phycol.* **15**: 135–141.

- NAGATA, T., AND D. L. KIRCHMAN. 1996. Bacterial degradation of protein adsorbed to model submicron particles in seawater. *Mar. Ecol. Prog. Ser.* **132**: 241–248.
- NELSON, J. R., C. A. CARLSON, AND D. K. STEINBERG. 2004. Production of chromophoric dissolved organic matter by Sargasso Sea microbes. *Mar. Chem.* **89**: 273–287.
- , AND S. GUARDA. 1995. Particulate and dissolved spectral absorption on the continental shelf of the southeastern United States. *J. Geophys. Res.* **100**: 8715–8732.
- NELSON, N. B., AND D. A. SIEGEL. 2002. Chromophoric DOM in the open ocean, p. 547–578. *In* D. A. Hansell and C. A. Carlson [eds.], *Biogeochemistry of marine dissolved organic matter*. Academic.
- , ———, AND A. F. MICHAELS. 1998. Seasonal dynamics of colored dissolved organic matter in the Sargasso Sea. *Deep-Sea Res. I* **45**: 931–957.
- NIVEN, S. E. H., P. E. KEPKAY, AND A. BORAIE. 1995. Colloidal organic carbon and colloids <sup>234</sup>Th dynamics during a coastal phytoplankton bloom. *Deep-Sea Res. II* **42**: 257–273.
- PRICE, N. M., G. I. HARRISON, J. C. HERING, R. J. HUDSON, B. PALENIK, AND F. M. M. MOREL. 1989. Preparation and chemistry of the artificial algal culture medium. *Aquac. Biol. Oceanogr.* **6**: 443–461.
- PROCTOR, L. M., AND J. A. FUHRMAN. 1991. Role of viral infection in organic particle flux. *Mar. Ecol. Prog. Ser.* **69**: 133–142.
- RATANATHANAWONGS, S. K., AND J. C. GIDDINGS. 1993. Particle size analysis using flow field-flow fractionation, p. 13–29. *In* T. Provder [ed.], *Chromatography of polymers: Characterization by SEC and FFF*. American Chemical Society.
- SANTSCHI, P. H., E. BALNOIS, K. J. WILKINSON, J. ZHANG, AND J. BUFFLE. 1998. Fibrillar polysaccharides in marine macromolecular organic matter as imaged by atomic force microscopy and transmission electron microscopy. *Limnol. Oceanogr.* **43**: 896–908.
- SIEGEL, D. A., AND A. F. MICHAELS. 1996. Quantification of non-algal light attenuation in the Sargasso Sea: Implications for biogeochemistry and remote sensing. *Deep-Sea Res. II* **43**: 321–345.
- STRAMSKI, D., E. BOSS, D. BOGUCKI, AND K. J. VOSS. 2004. The role of seawater constituents in light backscattering in the ocean. *Prog. Oceanogr.* **61**: 27–56.
- SUNDH, I. 1989. Characterization of phytoplankton extracellular products (PDOC) and their subsequent uptake by heterotrophic organisms in a mesotrophic forest lake. *J. Plankton Res.* **11**: 463–486.
- THURMAN, E. M. 1985. *Organic geochemistry of natural waters*. Kluwer Academic.
- TRANVIK, L. J., E. B. SHERR, AND B. F. SHERR. 1993. Uptake and utilization of “colloidal DOM” by heterotrophic flagellates in seawater. *Mar. Ecol. Prog. Ser.* **92**: 301–309.
- TWARDOWSKI, M. S., E. BOSS, J. M. SULLIVAN, AND P. L. DONAGHAY. 2004. Modeling the spectral shape of absorption by chromophoric dissolved organic matter. *Mar. Chem.* **89**: 69–88.
- VAILLANCOURT, R. D., AND W. M. BALCH. 2000. Size distribution of marine submicron particles determined by flow field-flow fractionation. *Limnol. Oceanogr.* **45**: 485–492.
- VODACEK, A., N. V. BLOUGH, M. D. DEGRANDPRE, E. T. PELTZER, AND R. K. NELSON. 1997. Seasonal variation of CDOM and DOC in the Middle Atlantic Bight: Terrestrial inputs and photooxidation. *Limnol. Oceanogr.* **42**: 674–686.
- WELLS, M. L. 2004. The colloidal size spectrum of CDOM in the coastal region of the Mississippi Plume using flow field-flow fractionation. *Mar. Chem.* **89**: 89–102.
- , AND E. D. GOLDBERG. 1991. Occurrence of small colloids in seawater. *Nature* **353**: 342–344.
- , AND ———. 1992. Marine submicron particles. *Mar. Chem.* **40**: 5–18.
- , AND ———. 1993. Colloid aggregation in seawater. *Mar. Chem.* **41**: 353–358.
- , AND ———. 1994. The distribution of colloids in the North Atlantic and Southern Oceans. *Limnol. Oceanogr.* **39**: 286–302.
- YACOBI, Y. Z., J. J. ALBERTS, M. TAKACS, AND M. McELVAINE. 2003. Absorption spectroscopy of colored dissolved organic carbon in Georgia (USA) rivers: The impact of molecular size distribution. *J. Limnol.* **62**: 41–46.
- YAMASAKI, A., H. FUKUDA, R. FUKUDA, T. MIYAJIMA, T. NAGATA, H. OGAWA, AND I. KOIKE. 1998. Submicrometer particles in northwest Pacific environments: Abundance, size distribution and biological origins. *Limnol. Oceanogr.* **43**: 536–542.
- ZANARDI-LAMARDO, E., C. D. CLARK, C. A. MOORE, AND R. G. ZIKA. 2002. Comparison of the molecular mass and optical properties of colored dissolved organic material in two rivers and coastal waters by flow field-flow fractionation. *Environ. Sci. Technol.* **36**: 2806–2814.
- , ———, AND R. G. ZIKA. 2001. Frit inlet/frit outlet flow field-flow fractionation: Methodology for colored dissolved organic material in natural waters. *Anal. Chim. Acta* **443**: 171–181.
- ZSOLNAY, A. 1979. Coastal colloidal carbon: A study of its seasonal variation and the possibility of river input. *Estuar. Coast. Mar. Sci.* **9**: 559–567.

Received: 28 March 2006

Accepted: 28 August 2006

Amended: 12 September 2006